

Hybrid Adaptive Control of an Active Multi-Focal Vision System

Alois Unterholzner and Hans-Joachim Wuensche

Abstract—Active multi-focal vision systems are designed to perform visual tasks such as saccades and smooth pursuit movements. Saccades are fast movements to a given position, which is a time-optimal control problem. Smooth pursuit movement is used to follow moving objects and is a tracking control problem. Therefore we use a hybrid approach for the control of our vision system. For saccades we use sliding-mode control with a switching line, designed such that nearly time-optimal control performance is achieved. For smooth pursuit movement we use state-space control to attain adequate tracking performance. To widen the applicability of our multi-focal vision system, it is designed such that cameras are easily exchangeable. Thus system dynamics is subject to change, which implies the need for adaptive control. This paper presents the design of the resulting hybrid adaptive controller together with experimental results.

I. INTRODUCTION

Visual perception is an important capability for autonomous systems. To exploit the advantages offered by tele-, wide-angle- or stereo-cameras, multi-focal vision systems are widely used. Moreover most multi-focal vision systems are active, e.g. pivotable in pitch and yaw axis and thereby enhance the field of view of the autonomous system, while limiting the amount of data to be processed. There is a rich body of literature discussing the design and control of multi-focal vision systems. To mention only a few: An overview, especially for humanoids, is given in [1] and [2]. The design of camera platforms for autonomous ground vehicles is discussed in [3] and [4].

An active vision system implies the need for visual behaviors such as saccades and smooth pursuit movements.

Smooth pursuit movements are used to track moving objects. That means the visual system has to follow a desired trajectory provided e.g. by a visual object tracking module. In [5] we achieved satisfactory results for the tracking problem with an adaptive state-space control law. For smooth pursuit movements we still use state-space control. Only minor modifications are necessary as the dynamic plant model has changed slightly.

Saccades are fast movements to a given position. In [5] the derived controller is also used for saccades. However fast saccades are only achievable if the actuator saturates, which implies that the control loop is no longer linear. There are three possible outcomes of using linear control – such as state-space control – for saccades: First, the controller gains are too small and the saccade is too slow. Secondly, the controller gains are too high and overshoot occurs. Thirdly, optimal controller gains, that are high enough but



Fig. 1. Two possible camera platform configurations

not too high, result in a near time-optimal saccade. However, the optimal controller gains are different for every saccade amplitude. An intuitive way to adjust the controller gains is to keep them low to avoid overshoot.

To overcome this limitation, saccades can be considered as a time-optimal control problem. Time-optimal control problems can be solved using Pontryagin's minimum principle [6], but the solution is sensitive to unknown plant dynamics or disturbances. Moreover it is difficult to derive a solution analytically for nonlinear systems. A robust adaptive proximate time-optimal solution for double integrator plants is given in [7].

Sliding-mode control is an inherently robust method to cope with uncertain plant dynamics. If the controlled system has reached the sliding-mode, it is insensitive to disturbances and system motion is determined by the sliding-surface only [8], [9]. Hyperplanes are used as sliding surfaces frequently. The system motion in sliding-mode is then governed by linear differential equations, with the drawback of a suboptimal transient response in terms of time-optimal control.

There are several approaches that try to utilize the robustness properties of sliding-mode control, while simultaneously attaining near time-optimal control performance, e.g. [10], [11] and [12]. In [10] a neural network is used to learn the time-optimal switching curve from actuator step responses. The resulting sliding-mode controller is combined with a PI-controller to achieve both good transient and steady state response. To achieve robust near time-optimal control, in [11] the combination of time-optimal control, sliding-mode control (with a hyperplane as sliding-surface) and a linearized feedback control is proposed. In [12] a nonlinear sliding-surface for a double integrator system is derived, that becomes identical to the time-optimal switching line in the limit. It is further analyzed how this switching surface has to be modified for nonlinear second-order systems. The necessary modifications lead to constraints, that prevent the sliding-surface from being time-optimal. Therefore a Takagi-Sugeno fuzzy-model is proposed to approximate a time-optimal sliding-surface.

The control law design methods described above are

offline methods and therefore only suitable for plants with constant parameters. Since the cameras of our vision system (Fig. 1) can be changed easily, plant parameters are not known in advance. If we want to derive near time-optimal saccades, we have to adapt the switching line according to online identified plant parameters. Our approach is to use the sliding-surface proposed in [12] and modify it to relax the necessary constraints. The resulting switching line is an implicit function, depending on the system state and the plant parameters. Therefore it can be adapted online.

The rest of the paper is organized as follows: The dynamic plant model is introduced in section II. Sections III and IV give a brief description of the applied state and parameter estimation. In section V the hybrid adaptive control law is presented. The main focus lies on the derivation of the sliding-surface. The switching strategy between state-space control and sliding-mode control is presented in this section as well. Experimental results are given in section VI. The paper concludes in section VII.

II. DYNAMIC MODEL

Plant dynamics is modelled as a nonlinear second-order differential equation [5]:

$$J \cdot \ddot{\varphi} = k_m \cdot I - \tau_\varphi - \tau_{\dot{\varphi}} \quad (1)$$

I is the torque generating motor current, k_m the motor torque constant and J the inertia of platform yaw axis. The angular velocity dependent disturbance torque $\tau_{\dot{\varphi}}$ is described by

$$\tau_{\dot{\varphi}} = \tau_c \cdot \text{sgn}(\dot{\varphi}) + d \cdot \dot{\varphi} \quad (2)$$

with τ_c representing Coulomb and d representing viscous friction coefficient; with $\text{sgn}(\cdot)$ being the signum function. The angular position dependent disturbance torque from [5] is augmented with a torsion-spring model $c \cdot \varphi$, since the disturbance torque resulting from twisted cables can no longer be neglected:

$$\tau_\varphi = r \cdot m \cdot g \cdot \sin(\theta_p) \cdot \cos(\varphi) + c \cdot \varphi \quad (3)$$

The term $r \cdot m \cdot g \cdot \sin(\theta_p) \cdot \cos(\varphi)$ describes the torque resulting from the unbalanced mass m w.r.t. the platform yaw axis. With distance r from the center of gravity of the unbalanced mass m to the center of rotation of the platform yaw axis, g gravitational acceleration and θ_p being the adjustable pitch angle of the platform yaw axis. The unbalanced mass results from the pitch axis encoder outweighing the pitch axis drive and any mass differences of the used camera/lens combinations. Defining $r \cdot m \cdot g \cdot \sin(\theta_p) =: \tau_u$, the disturbance torque τ_φ can be written as

$$\tau_\varphi = \tau_u \cdot \cos(\varphi) + c \cdot \varphi \quad (4)$$

With equations (2) and (4) the plant dynamics (1) can be summarized to

$$J \cdot \ddot{\varphi} = k_m \cdot I - d \cdot \dot{\varphi} - c \cdot \varphi - \tau_c \cdot \text{sgn}(\dot{\varphi}) - \tau_u \cdot \cos(\varphi) \quad (5)$$

III. PARAMETER ESTIMATION

Since the model parameters J , d , c , τ_c and τ_u are unknown, a parameter estimator is used to get estimates \hat{J} , \hat{d} , \hat{c} , $\hat{\tau}_c$ and $\hat{\tau}_u$ respectively. Discretizing equation (5) using the forward differences as suggested in [13]

$$\dot{\varphi} = (\varphi_{k+1} - \varphi_k) / T \quad (6)$$

we derive a discrete time plant model

$$\begin{aligned} \varphi_k &= -a_1 \cdot \varphi_{k-1} - a_2 \cdot \varphi_{k-2} + b_2 \cdot I_{k-2} \\ &\quad - \delta_1 \cdot \text{sgn}\left(\frac{\varphi_{k-1} - \varphi_{k-2}}{T}\right) - \delta_2 \cdot \cos(\varphi_{k-2}) \end{aligned} \quad (7)$$

which is linear in the parameters

$$a_1 = \frac{Td}{J} - 2, \quad a_2 = 1 - \frac{Td}{J} + \frac{cT^2}{J}, \quad b_2 = \frac{k_m T^2}{J} \quad (8)$$

$$\delta_1 = \frac{\tau_c T^2}{J}, \quad \delta_2 = \frac{\tau_u T^2}{J}$$

Then (7) can be written as linear regression and we are able to use a Recursive Least Squares (RLS) parameter estimator with parameter projection [14], [5].

IV. STATE ESTIMATION

Both state-space control and sliding-mode control require full state information. Therefore a state estimator is applied to derive full state information, using measured yaw axis position φ . Since the plant model (5) is nonlinear, we use parameter estimates $\hat{\tau}_c$ and $\hat{\tau}_u$ to compensate for the nonlinear disturbance terms in equation (5) with the disturbance feedforward

$$I_{ff} = k_m^{-1} \cdot (\hat{\tau}_c \cdot \text{sgn}(\dot{\varphi}) + \hat{\tau}_u \cdot \cos(\varphi)) \quad (9)$$

In [13] a similar approach is suggested for adaptive friction compensation. The plant input current I can be written as follows:

$$I = I_{ff} + I_{fb} + I_{ref} \quad (10)$$

with I_{ff} resulting from feedforward control, I_{fb} resulting from feedback control and I_{ref} resulting from reference input r . Inserting feedforward control (9) in the plant model (5) we get

$$\begin{aligned} J \cdot \ddot{\varphi} &= k_m \cdot (I_{fb} + I_{ref}) - d \cdot \dot{\varphi} - c \cdot \varphi \\ &\quad - (\tau_c - \hat{\tau}_c) \cdot \text{sgn}(\dot{\varphi}) - (\tau_u - \hat{\tau}_u) \cdot \cos(\varphi) \end{aligned} \quad (11)$$

Summarizing the remaining disturbance torques resulting from parameter estimation errors $\tau_u - \hat{\tau}_u$ and $\tau_c - \hat{\tau}_c$, as well as from unmodelled disturbances in one disturbance torque τ_d , equation (11) can be written as

$$J \cdot \ddot{\varphi} = k_m \cdot (I_{fb} + I_{ref}) - d \cdot \dot{\varphi} - c \cdot \varphi - \tau_d \quad (12)$$

We use $\dot{\tau}_d = 0$ as disturbance model, as this is found in [15] to be a good compromise between model complexity and estimation accuracy in the context of friction compensation.

Now we are able to derive a state estimator. Using the continuous time state-space formulation

$$\begin{aligned} \dot{x} &= Fx + G\bar{u}, \quad y = Cx, \quad \text{with} \\ x &= (\varphi, \dot{\varphi}, \tau_d, \dot{\tau}_d)^T, \quad \bar{u} = I_{fb} + I_{ref} \end{aligned} \quad (13)$$

we derive from equation (12) and disturbance model $\ddot{\tau}_d = 0$ the state-space description

$$F = \begin{pmatrix} 0 & 1 & 0 & 0 \\ -\frac{c}{J} & -\frac{d}{J} & -\frac{1}{J} & 0 \\ 0 & 0 & 0 & 1 \\ 0 & 0 & 0 & 0 \end{pmatrix}, G = \begin{pmatrix} 0 \\ \frac{k_m}{J} \\ 0 \\ 0 \end{pmatrix},$$

$$C = (1, 0, 0, 0) \quad (14)$$

As we are using a discrete time Kalman filter for state estimation, we need a discrete time description of (14):

$$x_{k+1} = Ax_k + B\bar{u}_k, y_k = Cx_k, \quad \text{with}$$

$$x_k = (\varphi_k, \dot{\varphi}_k, \tau_{dk}, \dot{\tau}_{dk})^T \quad (15)$$

Using (6) for discretization we get

$$A = \begin{pmatrix} 1 & T & 0 & 0 \\ -\frac{cT}{J} & \frac{J-Td}{J} & -\frac{T}{J} & 0 \\ 0 & 0 & 1 & T \\ 0 & 0 & 0 & 1 \end{pmatrix}, B = \begin{pmatrix} 0 \\ \frac{k_m T}{J} \\ 0 \\ 0 \end{pmatrix}$$

$$C = (1, 0, 0, 0) \quad (16)$$

Replacing parameters J , c and d at every time step k with their estimates \hat{J}_k , \hat{c}_k and \hat{d}_k , we get \hat{A}_k and \hat{B}_k as state- and input-matrices respectively.

V. CONTROLLER

Besides parameter- and state-estimator, the overall control architecture comprises a state-space and a sliding-mode controller together with a switching strategy, that decides which controller to use. Section V-A gives only a brief description of the derivation of the state-space control law, since the design is analog to [5]. The design of the adaptive sliding-mode control law is presented in section V-B in more detail. Finally a description of the switching strategy is given in section V-C.

A. State-Space Control

State-space control is used for smooth pursuit movements that demand a good tracking behavior. Therefore the reference r is designed to track the desired yaw angle φ_{ref} up to a ramp signal without steady state error. Thus r is a linear combination of φ_{ref} and its time derivative $\dot{\varphi}_{ref}$ with gains w_1 and w_2 :

$$r = w_1 \cdot \varphi_{ref} + w_2 \cdot \dot{\varphi}_{ref} \quad (17)$$

Following the controller design in [5], we define the discrete time tracking error $\varphi_{ref}(z) - \varphi(z)$ and calculate the steady state error, using the final value theorem. Provided \hat{c} and \hat{d} approach their true values, the steady state tracking error becomes zero if we choose

$$w_1 = k_1 + \frac{\hat{c}}{k_m} \quad \text{and} \quad w_2 = k_2 + \frac{\hat{d}}{k_m} \quad (18)$$

Using estimated state vector \hat{x}_k and disturbance feedforward I_{ff} together with discrete time reference input r_k , we get

the control law:

$$u_k = r_k - k_{1k} \hat{\varphi}_k - k_{2k} \dot{\hat{\varphi}}_k + \frac{\hat{\tau}_{dk}}{k_m} + \frac{\hat{\tau}_{ck}}{k_m} \operatorname{sgn}(\dot{\hat{\varphi}}_k) + \frac{\hat{\tau}_{wk}}{k_m} \cos(\hat{\varphi}_k) \quad (19)$$

Applying the control law (19) to the plant (5), we derive a second-order closed-loop system. As described in [5], controller gains k_1 and k_2 are determined by comparison of coefficients with the desired second-order closed-loop characteristic polynomial. We derive

$$k_1 = (\hat{J}\omega_0^2 - \hat{c})/k_m, \quad k_2 = (2\zeta\omega_0\hat{J} - \hat{d})/k_m \quad (20)$$

with closed-loop natural frequency ω_0 and damping ζ . Damping is chosen $\zeta > 1$ to avoid overshoot and ω_0 is calculated as follows [16],[5]:

$$\omega_0 = \frac{4.6}{\lambda\zeta\sqrt{\hat{J}}} \quad (21)$$

The constant λ is used to adjust the influence of estimated inertia \hat{J} on the desired closed-loop dynamics ω_0 .

B. Sliding-Mode Control

Saccadic movements are a typical application for time-optimal control. But, as already mentioned, time-optimal control is sensitive to plant uncertainties and disturbances. Moreover for nonlinear plants an analytic solution is difficult to derive. Therefore we use sliding-mode control with a sliding-surface $s = 0$ designed such that near time-optimal control performance is achieved.

The system motion of a system under sliding-mode control consists of two modes: the *reaching-mode* and the *sliding-mode* [9]. During the *reaching-mode* the phase trajectory of the system (Fig. 2) starts from anywhere in the phase plane and moves towards the switching surface $s = 0$. After reaching the sliding-surface $s = 0$ the phase trajectory will stay on it, provided the *reaching condition* is satisfied. Then the system is in the so called *sliding-mode* and the system motion is only governed by the differential equation $s = 0$. With the system under control

$$u = -K \operatorname{sgn}(s), \quad K > 0 \quad (22)$$

and using the Lyapunov function candidate

$$V(s) = \frac{1}{2}s^2 \quad (23)$$

a global reaching condition [9],[12] is given by

$$\dot{V}(s) = s\dot{s} < 0, \quad s \neq 0 \quad (24)$$

That means $s > 0$ indicates $\dot{s} < 0$ and vice versa. Thus the phase trajectories will always move towards and stay on $s = 0$ after reaching it.

In order to apply sliding-mode control, we rewrite plant dynamics (5) as a set of first order differential equations. Defining the control error $\varphi - \varphi_{ref} := e_1$ and noting that φ_{ref} is constant, we get

$$\begin{aligned} \dot{e}_1 &= e_2 \\ \dot{e}_2 &= (f(\dot{\varphi}) + g(\varphi) + h(\varphi, \dot{\varphi}) + u)/J \end{aligned} \quad (25)$$

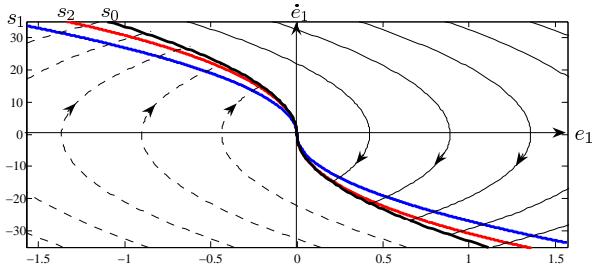


Fig. 2. Phase trajectories and sliding surfaces

with $\dot{e}_1 = \dot{\varphi}$ and $\dot{e}_2 = \ddot{\varphi}$. We separated the disturbance torque into three categories: $f(\dot{\varphi})$ describes the friction torque, with the property $f > 0$ if $\dot{\varphi} < 0$ and vice versa. Secondly $g(\varphi)$ is a spring torque and is assumed to be monotonically decreasing, that is $\partial g/\partial \varphi < 0 \forall \varphi$. Finally, $h(\varphi, \dot{\varphi})$ sums up the remaining disturbance torques that cannot be described by f or g . u is the plant input torque.

For a second-order system the nonlinear switching surface

$$s = \alpha e_1 + |e_2|e_2 = 0 \quad (26)$$

is proposed in [12]. Solving the differential equation (26) for constant α , the time span t needed to approach $e_1 = 0$ is calculated as follows:

$$t = 2\sqrt{|e_1(t=0)|/\alpha} \quad (27)$$

Provided that (24) is satisfied, it is obvious from (27) that the higher α is, the faster is the resulting transient response. To reach near time-optimal control α has thus to be maximized. For a double integrator plant switching surface, (26) becomes identical to the time-optimal switching line for $\alpha \rightarrow 2K$ [12], with K as the maximum control torque. In [12] it is argued that if the plant is not a pure double integrator but subject to disturbances, as e.g. system (25), the maximum values of the disturbances have to be considered in the calculation of α . Otherwise there are no resources left to compensate for the disturbances. Following this argumentation, it can be shown that the *reaching condition* (24) is satisfied for system (25) with control (22) and switching surface (26) for

$$\alpha < \frac{2}{J}(K - f_{max} - g_{max} - h_{max}) \quad (28)$$

But supposing that e.g. f describes viscous friction $f = d\dot{\varphi}$, f_{max} depends linearly on the largest possible angular velocity $\dot{\varphi}_{max}$. Thus α is too conservative for $\dot{\varphi} \ll \dot{\varphi}_{max}$.

In our approach we utilize the properties of the disturbance torques f and g to increase α , leading to a faster transient response of the control loop. We choose α as follows:

$$\alpha < \frac{2}{J}(K + g \cdot \text{sgn}(e_1) - h_{max}) \quad (29)$$

The term $g \cdot \text{sgn}(e_1)$ is chosen such that α increases if g reduces acceleration or supports deceleration. On the contrary α decreases if g supports acceleration or reduces deceleration. The friction torque f always counteracts the actuator torque and can thus be neglected in the calculation of α . Therefore α is independent from f_{max} and g_{max} , which is a desirable property. Fig. 2 depicts some switching surfaces

of system (25) with $\varphi_{ref} = 0$. The time-optimal switching surface is s_0 . s_1 and s_2 are the switching surfaces from (26) with α according to (28) or (29) respectively. s_2 lies inbetween s_0 and s_1 , indicating that using (29) to calculate α yields a faster transient response than using (28).

To verify if the *reaching condition* (24) is satisfied for the sliding-surface (26) with α chosen as in (29), we first calculate \dot{s} . Noting that $|e_2|$ can be written as $e_2 \cdot \text{sgn}(e_2)$ we derive

$$\dot{s} = \dot{\alpha}e_1 + \alpha e_2 + 2|e_2|\dot{e}_2 \quad (30)$$

with

$$\dot{\alpha} = \frac{2}{J} \cdot \frac{\partial g}{\partial \varphi} \cdot \frac{\partial \varphi}{\partial t} \cdot \text{sgn}(e_1) = \frac{2}{J} \cdot g' \cdot e_2 \cdot \text{sgn}(e_1) \quad (31)$$

Inserting (31), (25) and (22) in (30), we get

$$\begin{aligned} \dot{s} &= \frac{2}{J} [g'e_2|e_1| \\ &\quad + e_2(K + g \cdot \text{sgn}(e_1) - h_{max}) \\ &\quad + |e_2|(f + g + h - K\text{sgn}(s))] \end{aligned} \quad (32)$$

With control (22) acceleration \dot{e}_2 is negative for $s > 0$ and vice versa, since the maximum control torque K has to exceed the sum of the disturbances. Therefore all phase trajectories arrive finally in the second or fourth quadrant of the phase plane (Fig. 2). It is sufficient then to evaluate equation (32) only in quadrant II and IV. For the area $s > 0$, $e_1 < 0$ and $e_2 > 0$ we get

$$\dot{s} = \frac{2}{J}e_2(g'|e_1| + f + h - h_{max}) < 0 \quad (33)$$

and therefore $s\dot{s} < 0$, since $f < 0$ for $e_2 > 0$, $h < h_{max}$ and $g' < 0$. For $s < 0$, $e_1 > 0$ and $e_2 < 0$, we derive

$$\dot{s} = -\frac{2}{J}e_2(-g'|e_1| + f + (h + h_{max})) > 0 \quad (34)$$

Again $s\dot{s}$ is negative due to the properties of f , g' and h . The *reaching condition* (24) is satisfied for both areas $s > 0$, $e_1 > 0$, $e_2 < 0$ and $s < 0$, $e_1 < 0$, $e_2 > 0$, if the restriction

$$-g'|e_1| < 2(K - h_{max}) - f_{max} \quad (35)$$

holds. As a consequence, the system (25) with control (22) using sliding-surface (26), with α chosen as in (29), reaches the *sliding-mode* if restriction (35) is satisfied.

Comparing system (25) with the plant dynamics (5) we get

$$\begin{aligned} f &= -d \cdot \dot{\varphi} - \tau_c \cdot \text{sgn}(\dot{\varphi}) \\ g &= -c \cdot \varphi \\ h &= -\tau_u \cdot \cos(\varphi) \end{aligned} \quad (36)$$

for the disturbance torques f , g and h . The maximum control torque K in (22) corresponds to the maximum actuator torque $k_m \cdot I_{max}$. Using the disturbance torques from (36) and noting that $e_{1,max} = 2\varphi_{max}$, we can rewrite inequation (35) as follows:

$$g_{max} + h_{max} + f_{max} < K \quad (37)$$

This is not a major restriction since in practice the maximum actuator torque has to be higher than the sum of all disturbances.

Since we do not know the plant parameters in advance, we use the parameter estimates derived from the RLS parameter estimator described in section III. Moreover we use the state estimates provided by the Kalman filter introduced in section IV. Thus the sliding-surface is

$$s = \alpha(\hat{\varphi}_k - \varphi_{ref}) + |\dot{\hat{\varphi}}_k| \dot{\hat{\varphi}}_k \quad (38)$$

with

$$\alpha < \frac{2}{J}(K - \hat{c} \cdot \hat{\varphi}_k \cdot \text{sgn}(\hat{\varphi}_k - \varphi_{ref}) - |\hat{\tau}_u|) \quad (39)$$

The controller output is a square wave with time varying period. Square waves can be considered to be the sum of their harmonics. Therefore the input signal of the parameter estimator is persistently exciting and the estimated parameters will approach their true values. Then the estimated disturbance torque $\hat{\tau}_d$ is zero and the state estimates are close to the true states (sec. IV). Thus the *reaching condition* for plant (5) with the sliding-surface determined by (38) and (39) is satisfied.

It is obvious from the phase plane (Fig. 2) that all the sliding surfaces have negative slopes. Therefore a second-order system under control (22) is always stable even if the *reaching condition* is not satisfied and the *sliding-mode* is never reached. This is also true for the transient time while the parameter estimates have not converged.

The stability of the proposed adaptive sliding-mode control is established this way.

C. Switching Strategy

To switch between state-space control and sliding-mode control the simple hysteresis

$$\begin{aligned} \text{IF } |\varphi_{ref} - \varphi| > \epsilon_u \quad \text{THEN } \text{saccade} &= \text{true} \\ \text{IF } |\varphi_{ref} - \varphi| < \epsilon_l \quad \text{THEN } \text{saccade} &= \text{false} \end{aligned}$$

is used, with $\epsilon_u > \epsilon_l > 0$. If the control error $\varphi_{ref} - \varphi$ exceeds the upper threshold ϵ_u , a saccade is carried out and sliding-mode control is active. If the control error goes below the lower threshold ϵ_l , state-space control becomes active until the control error exceeds ϵ_u again.

VI. EXPERIMENTAL RESULTS

For our experiments we used the two configurations of our camera platform shown in Fig. 1. This configurations equipped with three (Fig. 1(a)) and five cameras (Fig. 1(b)) are called 3c- and 5c-configuration respectively. Our experiments focus on saccades, as the main purpose of the proposed hybrid control approach is to derive saccades that are close to time-optimal and avoid overshooting. Saccades with three different step sizes were conducted. For every step size we compared the results of the proposed sliding-mode control with the previously used state-space control. The step sizes were $\pm 10^\circ$, $\pm 20^\circ$ and $\pm 30^\circ$ (Fig. 3). Every plot of Fig. 3 depicts four saccades: two for each platform configuration,

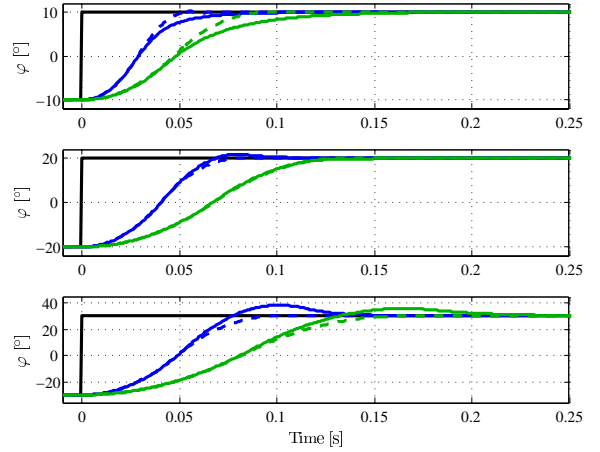


Fig. 3. Saccades: Black lines are reference values. Blue lines correspond to the 3c-configuration, green lines to the 5c-configuration. The dashed lines result from sliding-mode control, the solid lines from state-space control.

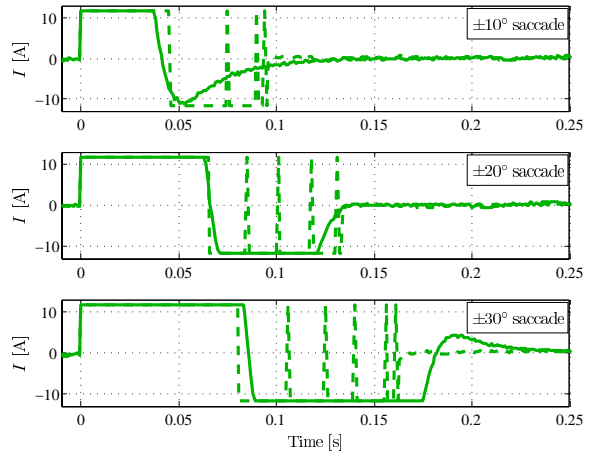


Fig. 4. Controller output for saccades of the 5c-configuration: Solid lines correspond to state-space control, dashed lines to sliding-mode control.

resulting from sliding-mode control and state-space control respectively.

For fast saccades maximum acceleration followed by maximum deceleration is required. Sliding mode control design is explicitly based on the maximum achievable acceleration and deceleration. That is why sliding-mode control suits saccadic movements better than state-space control.

From Fig. 3 it is obvious, that saccades under state-space control are either too slow or result in overshoot. The results for sliding-mode and state-space control are similar only for a small operating range as can be seen from the $\pm 20^\circ$ -saccade.

Fig. 4 depicts the controller output corresponding to the saccades of the 5c-configuration shown in Fig. 3. The switching activity (chattering) of the sliding-mode controller is low, indicating that the control performance is close to time-optimal. For the $\pm 20^\circ$ -saccade the controller output of state-space control and sliding-mode control overlap to a large extent. In particular the switching from acceleration to deceleration and vice versa takes place at nearly identical points in time. Therefore the resulting saccades are also similar. During the $\pm 30^\circ$ -saccade the state-space control output changes from acceleration to deceleration later than the sliding-mode control output. Also the deceleration phase

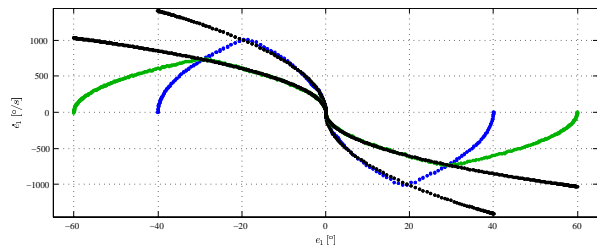


Fig. 5. Sliding surfaces and phase trajectories: The blue line corresponds to the phase trajectory of the 3c-configuration, the green line to the trajectory of the 5c-configuration. The black lines are the corresponding sliding surfaces.

is finished later, resulting in considerable overshoot. For the $\pm 10^\circ$ -saccade the state-space controller starts decelerating earlier than the sliding-mode controller and thus the corresponding saccade is finished later.

The sliding surfaces for the 3c- and 5c-configuration are shown in Fig. 5. Note that the slope of the sliding-surface of the 3c-configuration is higher than the slope of the 5c-configuration. This results mainly from the influence of the estimated inertia \hat{J} on the calculation of α in equation (39). Obviously the inertia of the 3c-configuration is smaller than the inertia of the 5c-configuration.

Moreover the resulting phase trajectories of the $\pm 20^\circ$ -saccade for the 3c-configuration and the $\pm 30^\circ$ -saccade for the 5c-configuration are depicted in Fig. 5. After reaching the sliding-surface, the trajectories stay in a small vicinity of the surface, due to the non-ideal components of a real-world control-loop.

A sawtooth signal is used as position reference to test the switching between sliding-mode control and state-space control (Fig. 6). With the sawtooth signal saccades and smooth pursuit movements can be simulated since it offers fast (saccade like) changes as well as continuous change over time with a constant slope. The output of the switching hysteresis proposed in section V-C is depicted in red. Both smooth pursuit movements and saccades show satisfactory control behavior. Furthermore the switching between both controllers is smooth and without noticeable influence on the control performance.

VII. CONCLUSION

In this paper a hybrid adaptive control strategy for an active multi-focal vision system is presented. Saccades and smooth pursuit movements are basic capabilities of an active vision system. Since this leads to different requirements for the controller, a hybrid approach is proposed. Sliding mode control is used for saccades and state-space control for smooth pursuit movements. A simple hysteresis is sufficient to switch reliably between both controllers. Moreover the cameras of the vision system can be changed easily to improve its applicability. As a consequence system dynamics may vary. Therefore the controller adapts itself to different plant dynamics. Compared to using state-space control only, the proposed hybrid control strategy shows superior performance for saccadic movements. It is faster for small saccades and no overshoot occurs for large saccades.

The low switching activity of the proposed sliding-mode

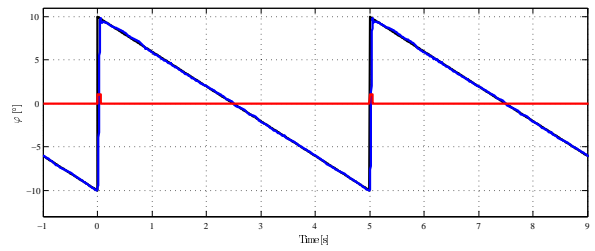


Fig. 6. Saccades and smooth pursuit movements: The black line is the reference value. The blue line corresponds to the 3c-configuration. The red line states which control law is active, state-space or sliding-mode control

control law indicates that near time optimality is achieved. However improvements may be possible by further relaxing the constraints preventing the switching surface from being time-optimal. Apart from possible modifications of the switching surface, it should be investigated how chattering could be avoided completely. Applying some of the well known techniques to reduce chattering, may serve as a starting point.

REFERENCES

- [1] K. Kühnlenz, M. Bachmayr, and M. Buss, "A Multi-Focal High-Performance Vision System," *Proceedings of the 2006 IEEE International Conference on Robotics and Automation*, pp. 150–155, 2006.
- [2] K. Kühnlenz, "Aspects of Multi-Focal Vision," Dissertation, Technische Universität München, München, 2006.
- [3] E. D. Dickmanns, "An advanced vision system for ground vehicles," in *Proceedings of the 1st International Workshop on 'In-Vehicle Cognitive Computer Vision Systems'*, Graz, Austria, April 2003.
- [4] —, *Dynamic Vision for Perception and Control of Motion*. London: Springer, 2007.
- [5] A. Unterholzner and H.-J. Wuensche, "Adaptive State Space Control of a Camera Platform for an Autonomous Ground Vehicle," in *Proceedings of the 2009 IEEE Intelligent Vehicles Symposium*, Xi'an, China, June 2009.
- [6] M. Athans and P. L. Falb, *Optimal Control: An Introduction to the Theory and Its Applications*. New York: McGraw-Hill, Inc., 1966.
- [7] G. F. Franklin, J. D. Powell, and M. Workman, *Digital Control of Dynamic Systems*, 3rd ed. Menlo Park, California: Addison Wesley Longman, 1998.
- [8] V. I. Utkin, "Variable Structure Systems with Sliding Modes," *IEEE Transactions on Automatic Control*, vol. AC-22, no. 2, pp. 212–222, 1977.
- [9] J. Y. Hung, W. Gao, and J. C. Hung, "Variable structure control: A survey," *IEEE Transactions on Industrial Electronics*, vol. 40, no. 1, pp. 2–22, February 1993.
- [10] T. Chatchanayuenyong and M. Parnichkun, "Time Optimal Hybrid Sliding Mode-PI Control for an Autonomous Underwater Robot," *International Journal of Advanced Robotic Systems*, vol. 5, no. 1, pp. 91–98, 2008.
- [11] K. H. You and E. B. Lee, "Robust, Near Time-Optimal Control of Nonlinear Second Order Systems with Model Uncertainty," in *Proceedings of the 2000 IEEE International Conference on Control Applications*, September 2000.
- [12] B. Iliev and I. Kalaykov, "Minimum-time sliding mode control for second-order systems," in *Proceedings of the 2004 American Control Conference*, June 2004.
- [13] C. Canudas, K. J. Åström, and K. Braun, "Adaptive Friction Compensation in DC-Motor Drives," *IEEE Journal of Robotics and Automation*, vol. RA-3, No. 6, pp. 681–685, 1987.
- [14] G. C. Goodwin and K. S. Sin, *Adaptive Filtering Prediction And Control*, ser. Information and System Sciences, T. Kailath, Ed. Engelwood Cliffs, New Jersey 07632: Prentice-Hall, Inc, 1984.
- [15] A. Ramasubramanian and L. R. Ray, "Comparison of EKBF-based and Classical Friction Compensation," *Journal of Dynamic Systems, Measurement, and Control*, vol. 129, pp. 236–242, 2007.
- [16] G. F. Franklin, J. D. Powell, and A. Emami-Naeini, *Feedback Control of Dynamic Systems*, 4th ed. Upper Saddle River, New Jersey: Prentice Hall, 2002.